Nano Energy 102 (2022) 107670

Contents lists available at ScienceDirect

Nano Energy

journal homepage: www.elsevier.com/locate/nanoen

Scalable and sustainable wood for efficient mechanical energy conversion in buildings via triboelectric effects☆

Jianguo Sun [a,b], Urs Schütz [c], Kunkun Tu [a,b], Sophie Marie Koch [a,b], Günther Roman [d,e], Sandro Stucki [a,b], Feng Chen [a,b], Yong Ding [a,b], Wenqing Yan [a,b], Changsheng Wu [f], Laura Stricker [g], Ingo Burgert [a,b], Zhong Lin Wang [h], Dirk Hegemann [c,*], Guido Panzarasa [a,b,**]

[a] Wood Materials Science, Institute for Building Materials, ETH Zürich, 8093 Zürich, Switzerland
[b] WoodTec Group, Cellulose & Wood Materials, Empa, 8600 Dübendorf, Switzerland
[c] Plasma & Coating Group, Advanced Fibers, Empa – Swiss Federal Laboratories for Materials Science and Technology, 9014 St. Gallen, Switzerland
[d] Laboratory of Adhesives and Polymer Materials, Institute of Materials and Process Engineering, Zurich University of Applied Sciences, 8401 Winterthur, Switzerland
[e] Laboratory for Multifunctional Materials, Department of Materials, ETH Zürich, 8093 Zürich, Switzerland
[f] Department of Materials Science Engineering, National University of Singapore, 117575, Singapore
[g] Soft Materials, Department of Materials, ETH Zürich, 8093 Zürich, Switzerland
[h] School of Materials Science and Engineering, Georgia Institute of Technology, Atlanta, GA 30332, United States

ARTICLE INFO

Keywords:
Wood
Triboelectric
Plasma treatment
Energy-efficient buildings
Sustainability

ABSTRACT

Triboelectric nanogenerators (TENG) have great potential to help enhancing the energy efficiency of buildings, and thus to contribute significantly to the reduction of global greenhouse gas emissions. However, there are major barriers against the adoption of such emerging energy technologies. Meeting the need for sustainable large-scale fabrication of high-performance products remains a critical challenge towards real-world TENGs' building applications. To mitigate this challenge, we enhance the poor polarizability of native wood by a scalable plasma treatment, a facile approach which to the greatest degree preserves wood's warm colors, mechanical robustness while efficiently enhancing the triboelectric output. We demonstrate the enhancement of electric output by assembling wood triboelectric nanogenerators (W-TENGs) in both contact-separation and single-electrode operation modes. We show that when two radial-cut wood samples (L × R × T: 100 × 80 × 1 mm^3), one treated with an O_2 plasma and the other with a $C_4F_8 + O_2$ plasma, are subjected to periodic contact and separation with an applied pressure as low as 0.0225 MPa, a maximum voltage of 227 V and a current of 4.8 μA are produced. Eventually, we showcase the real-world applicability of our approach with two prototypes of triboelectric wood floors, opening up new technological pathways towards a 'net-zero emissions' future.

1. Introduction

Buildings account for approximately 40% of the total world energy consumption [1–3]. Conventional buildings use up to 50% of the energy for heating, cooling, ventilation, and lighting purposes. Thus, improving the energy efficiency of buildings worldwide is key to reduce global greenhouse gas emissions. Current approaches mainly focus on reducing energy consumption, *e.g.,* by improving thermal insulation and sunlight harvesting, as well as by promoting natural lighting [3,4]. Active energy generation by direct conversion of renewable energy sources into electricity is another promising direction to make buildings energy-neutral or even energy-positive entities [5,6]. However, there are major barriers for the integration of emerging energy technologies into buildings. For example, current technology focuses on installing large photovoltaic panels on roofs, which can affect the building's aesthetic appearance and whose efficiency is limited by weather conditions [6,7]. Ideally, the

☆ Prof Zhong Lin Wang, an author on this paper, is the Editor-in-Chief of Nano Energy, but he had no involvement in the peer review process used to assess this work submitted to Nano Energy. This paper was assessed, and the corresponding peer review managed by Professor Chenguo Hu, also an Associate Editor in Nano Energy.

* Corresponding author.
** Corresponding author at: Wood Materials Science, Institute for Building Materials, ETH Zürich, 8093 Zürich, Switzerland.
E-mail addresses: dirk.hegemann@empa.ch (D. Hegemann), guido.panzarasa@ifb.baug.ethz.ch (G. Panzarasa).

https://doi.org/10.1016/j.nanoen.2022.107670
Received 17 June 2022; Received in revised form 26 July 2022; Accepted 2 August 2022
Available online 4 August 2022

construction materials themselves should be enabled to actively produce electricity from those renewable sources, *e.g.* mechanical energy, which are not limited by weather conditions. Only then, future buildings could self-decarbonize without restrictions and preserving their aesthetic appearance.

Wood has been used by humans for thousands of years as a construction material owing to its remarkable mechanical properties, low-cost, sustainability and aesthetic appearance [8]. Beyond structural applications, wood was recently modified by chemical and/or physical treatment for functional energy-saving applications [9]. For instance, optically transparent wood is an emerging candidate for replacement of traditional windows for light management in smart buildings [10–12]. Regarding thermal management, wood was modified to improve thermal insulating and radiative cooling properties [2,13]. In addition, wood could also contribute to active power generation in buildings when exploited as a triboelectric material. Triboelectric nanogenerators (TENGs) enable the direct conversion of mechanical energy into electricity based on the coupling effects of contact electrification and electrostatic induction [14–18]. Depending on their chemical composition and structure, a variety of materials can display a more-or-less high tendency to gain (*e.g.* poly(tetrafluoroethylene), PTFE) or loose (*e.g.* Nylon) electrons, resulting in an empirical triboelectric series [19,20]. Native wood occupies a nearly central position in the triboelectric series, which explains the limited progress made so far in the design of W-TENGs [21,22]. Although recently several kinds of wood-based TENGs have been proposed [8,23–28], they usually make use of highly polarizable, but unsustainable, triboelectric materials to maximize the electrical output. The overall proportion of wood used in such devices is small, consequently reducing the benefits associated with the use of wood itself. Such wood-TENGs (W-TENGs) have high materials and fabrication costs and/or have low environmental friendliness, making them unsuitable for large-scale building applications [23,24]. Moreover, the use of relatively time-consuming and complex synthetic processes increases the manufacturing costs and reduces scalability [23,25]. Last but not least, those previous works contribute little insight on how to tune the tribo-polarity of wood itself without compromising on sustainability aspects.

Here we propose a convenient solution to the existing challenges, which could help promote the commercial fabrication and real-world applicability of TENGs. In this work, we used plasma treatments to rationally tune the triboelectric properties of wood itself. Our results showed that wood acquires a higher tendency to become positively charged during friction after an O_2 plasma treatment, while a $C_4F_8 + O_2$ plasma treatment makes wood more tribonegative. Thanks to this enhanced difference of triboelectric polarities we could fabricate efficient W-TENGs made almost entirely of plasma-treated wood. We demonstrate two designs of self-powered triboelectric wood floors, contact-separation and single-electrode mode. Besides powering traditional electronic devices (such as light emitting diodes LEDs and liquid crystal displays LCDs), our scalable wood-TENG can generate enough power to activate a miniature electrochromic window, useful to modulate sunlight transmittance into buildings as well as to improve the thermal comfort of the occupants [29–31]. Compared to previous studies, this molecular-level surface modification ensures an active contribution of wood to the triboelectrification process, providing sufficient insights for moving wood across the triboelectric series and unlocking its potential for multi-level energy needs. Our new approach minimizes the use of non-sustainable and expensive materials, to the greatest degree preserving beneficial features of wood (*e.g.* aesthetic appearance and mechanical robustness) while maximizing the triboelectric output. Furthermore, it is fast, convenient, and solvent-free, making it highly suitable for industrial-level production and eventually for large-scale building applications. With these compelling advantages, our study provides insight on how to unlock the potential of wood for triboelectric energy generation, a substantial step towards developing next-generation energy-efficient buildings.

2. Results and discussion

Increasing the surface contact area and/or introducing chemical groups with improved electron-transfer ability are conventional strategies to enhance the electrical output of TENGs [32,33]. Previous surface modification approaches were mainly based on wet chemistry and surface replication, with limitations in size control and often poor scalability [33,34]. In contrast, plasma (an excited gas consisting of a complex mixture of electrons, ions, atoms/molecules, and free radicals) treatment is an extremely versatile approach for surface modification, dry (solvent-free) and easily scalable at the industrial level. Besides, depending on the conditions of the plasma (*e.g.* gas composition, pressure, power, treatment time), it is possible to generate chemical and morphological changes on the materials' surface, leaving the bulk intact [20,35–37]. Unlike other natural and synthetic materials, deeper insight into the treatment process and its impact on the properties of bulk wood are still needed, owing to its complex nature. In addition, the triboelectric properties of wood after plasma treatment have never been explored before.

Spruce (*Picea abies*) was selected for the present study as one of the most common wood species in central Europe, widely used for building applications. A piece of native spruce veneer (20 mm × 35 mm × 1 mm) shows only a weak tendency to donate or acquire electrons during the triboelectrification process due to its neutral relative polarity. To rationally tune and improve the negligible polarizability of wood, we treated it with different plasmas, as illustrated in Fig. 1a. Spruce veneers were exposed either to O_2 plasma or a mixed $C_4F_8 + O_2$ plasma, resulting in surface morphological and/or chemical modifications. Thanks to its enhanced polarity, plasma-treated spruce exhibited a higher tendency to donate or acquire electrons. In the following, we undertook a detailed exploration of the surface of wood and of its morphological and chemical modifications as a function of plasma composition, power and time of treatment, as well as wood cutting direction and method.

The effects of these two plasma treatments on the surface morphology of wood were evaluated by means of scanning electron microscopy (SEM). As shown in Fig. 1b-c and Fig. S1, native wood veneers cut in different planes (cross-section, tangential and radial) show different morphologies and structures, thanks to the intrinsic anisotropy of wood. Cross-section veneers cut by circular saw have channels (lumina) filled with cell wall fragments. Laser-cutting was applied to obtain veneers with clean cross-sections, leading to relatively smooth surfaces with open lumina and the characteristic porous structure [38]. On the other hand, the wood structure of saw-cut radial and tangential sections are much better preserved, with only a few fragments visible on the surface.

Compared to the relatively homogeneous and smooth surface of native wood, the surface of wood samples treated by O_2 plasma (5 min at 5 Pa and 60 W, 20 sccm gas flow rate) is more inhomogeneous and rougher, with numerous visible voids or grooves (Fig. 1d, e and Fig. S2). This pronounced change in surface morphology can be attributed to an anisotropic degradation of wood resulting from its interaction with the energetic plasma, leading to the formation of volatile products (such as water vapor and carbon dioxide). At the same time, the surface is enriched with polar groups (*e.g.* hydroxyl, carbonyl) resulting from chemical reactions [39].

Plasmas based on C_4F_8 are conventionally used to grow fluorocarbon polymer films, which are simple, efficient and reproducible. The addition of a small amount of O_2 allows to direct the polymerization process and the resulting surface functionalization with fluorine-rich groups [40,41]. A mixture of C_4F_8 (18.0 sccm) and O_2 (2.0 sccm) was then used as plasma source, keeping other parameters (pressure, power, and time as well as total gas flow rate) the same as for the pure O_2 plasma treatment. Fig. 1f, g and Fig. S2 show that, unlike the O_2 plasma, the treatment with $C_4F_8 + O_2$ plasma has no visible effect on the surface morphology of wood, which appears unaltered.

Increasing the surface roughness of triboelectric materials leads to a

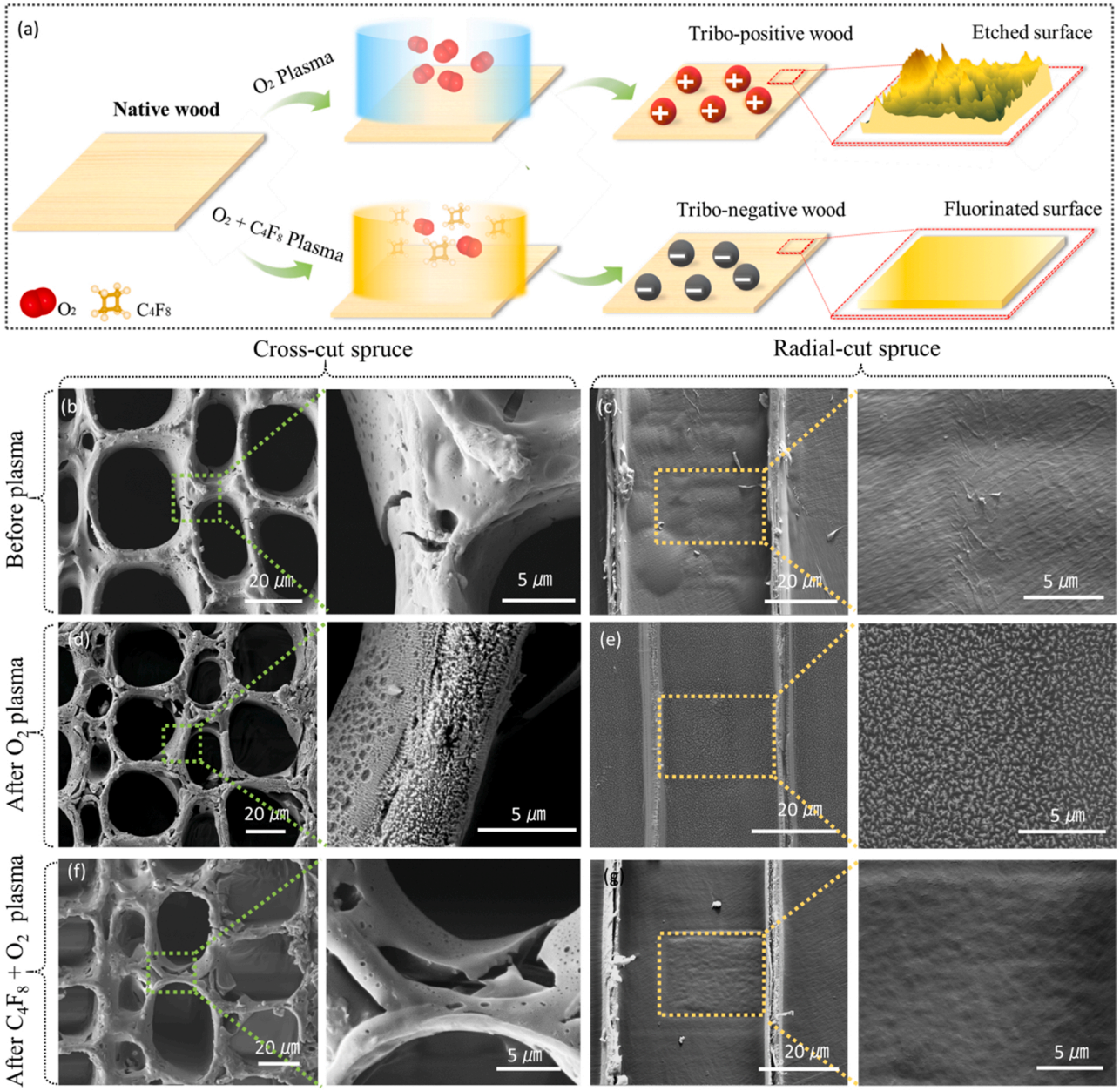

Fig. 1. Schematic illustration of plasma treatment of wood and its effect on wood's surface morphology. **(**a) Schematic representation of wood plasma treatment. (b-g) Representative SEM images of (b, d, f) cross-cut veneer (cut by laser, L × R × T: 1 mm × 35 mm × 20 mm) and (c, e, g) radial-cut veneer (cut by saw, L × R × T: 35 mm × 20 mm ×1 mm). (b) Representative SEM images of native cross-cut veneer. (c) Representative SEM images of native radial-cut veneer. (d) Representative SEM images of cross-cut veneer after O_2 plasma treatment. (e) Representative SEM images of radial-cut veneer after O_2 plasma treatment. (f) Representative SEM images of cross-cut veneer after $C_4F_8 + O_2$ plasma treatment. (g) Representative SEM images of radial-cut veneer after $C_4F_8 + O_2$ plasma treatment.

higher effective surface area, enhancing TENG's performance [17,42]. However, excessive roughness may induce tip-to-tip incomplete contact between the surfaces, decreasing the electrical output [43]. To optimize the amount of transferred charges between two triboelectric materials, the surface roughness should be controlled in a proper range. Fig. 2a–d show 3D surface profiling images of different sections of native wood, respectively: cross (cut by laser), cross (cut by saw), tangential (cut by saw), and radial (cut by saw). The average roughness (Ra) values for cross-section veneer cut by laser and saw are, respectively, 11.59 and 7.47 μm (Table S1). The much higher Ra of laser-cut wood may result from the highly porous structure. The Ra values for tangential and radial veneer sections are 6.33 and 8.91 μm, respectively. These Ra parameters are representative of the inherent roughness of the different wood surfaces, originating from the specific arrangement of microscale cells, which will contribute different electrical output performances when assembled in a TENG.

Nanoscale roughness changes produced by the plasma treatments were explored by atomic force microscopy (AFM). These investigations were performed on the cell wall inside cut-open cells of radial-cut samples. As shown in Fig. 2e, native radial saw-cut veneer has a relatively low Ra of 2.84 nm and root mean square roughness (Rq) of 3.86 nm, respectively. The 3D AFM topographic image in Fig. 2f shows that the surface of wood treated by O_2 plasma (60 W, 5 min) is greatly roughened at the nanoscale, with a much higher Ra of 46.57 nm and Rq of 57.48 nm, respectively. Increasing the O_2 plasma treatment time to 15 min (power constant at 60 W), the Ra and Rq of wood surface are increased respectively to 70.71 nm and 92.18 nm, as shown in Fig. S3 and Table S2. Consistent with the SEM results, the surface morphology

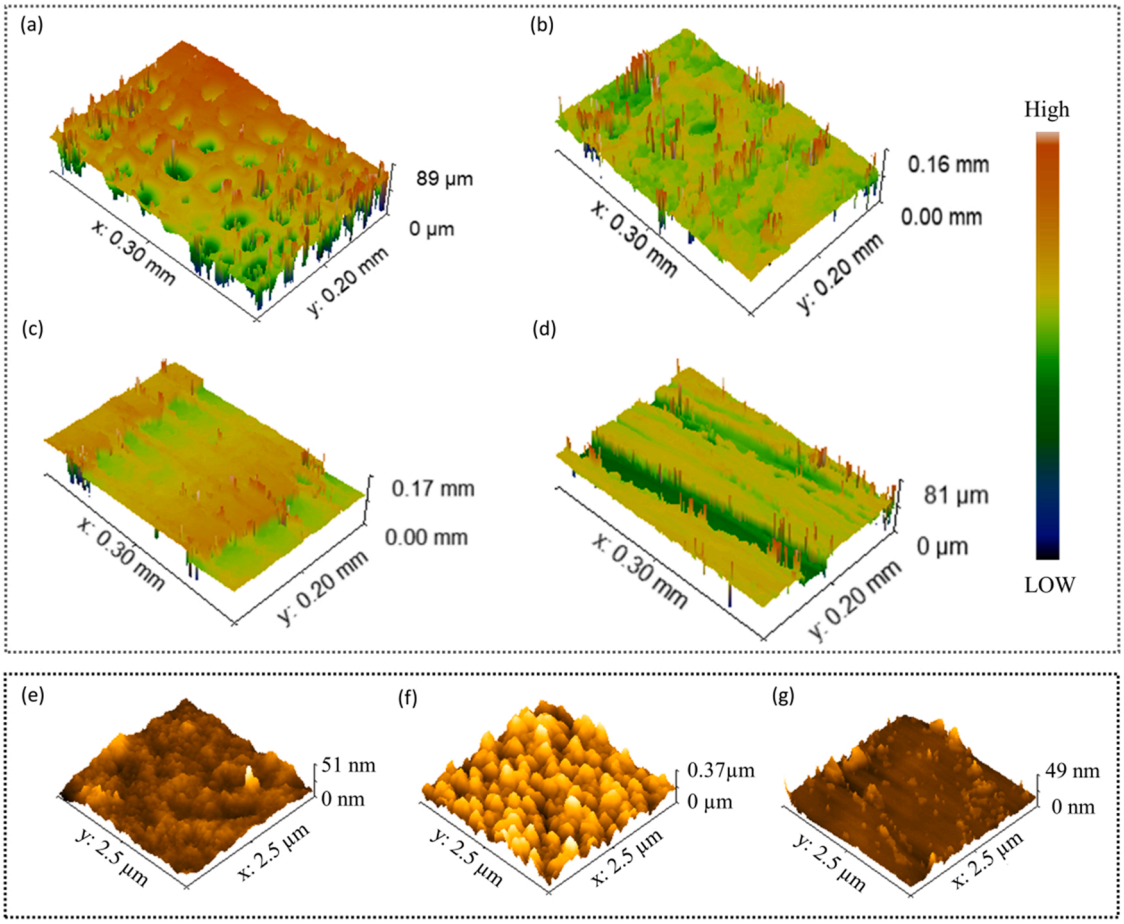

Fig. 2. Surface roughness of native wood and plasma-treated wood. (a) 3D surface profiles obtained by stylus surface profilometry for cross-cut veneer (cut by laser, L × R × T: 1 mm × 35 mm × 20 mm). (b) 3D surface profiles obtained by stylus surface profilometry for cross-cut veneer (cut by saw, L × R × T: 1 mm × 35 mm × 20 mm). (c) 3D surface profiles obtained by stylus surface profilometry for tangential-cut veneer (cut by saw, L × R × T: 35 mm × 1 mm × 20 mm). (d) 3D surface profiles obtained by stylus surface profilometry for radial-cut veneer (cut by saw, L × R × T: 35 mm × 20 mm × 1 mm). (e) AFM results for native wood (radial cut, L × R × T: 35 mm × 20 mm × 1 mm). (f) AFM results for O_2 plasma-treated wood (60 W, 5 min) (radial cut, L × R × T: 35 mm × 20 mm × 1 mm). (g) AFM results for $C_4F_8 + O_2$ plasma-treated wood (60 W, 5 min) (radial cut, L × R × T: 35 mm × 20 mm × 1 mm).

of wood treated by the $C_4F_8 + O_2$ plasma (60 W, 5 min) is much more similar to that of native wood, as shown in Fig. 2g. Both Ra and Rq values, respectively of 2.01 nm and 3.11 nm, are comparable to those of native wood, which retained also for prolonged treatment time (Fig. S3 and Table S2). These results indicate that the O_2 plasma treatment plays an important role by improving the effective contact area of the wood surface, while the mixed $O_2 + C_4F_8$ plasma treatment preserves the surface morphology of native wood.

Surface chemical changes before and after the two plasma treatments were identified by X-ray photoelectron spectroscopy (XPS). Fig. 3a shows the survey spectra for native wood. The deconvolution of O 1 s and C 1 s peaks gives a composition of 50.3% C–C, 38.0% C–O and 11.7% C═O bonds, respectively (Fig. 3b), in agreement with the average molecular composition of wood.

After O_2 plasma treatment, which was performed at 60 W for 5 min, the C–C peak areas increased, while the C═O carbonyl groups diminished. There is an increase in hydroxyl/ether C-O as well as of carboxyl/ester O-C═O groups, these latter amounting to 1.7% (Fig. 3c, 3d and Fig. S4). Traces of fluorine and calcium were also found in the spectrum of O_2 plasma-treated wood, most probably originating from a contamination in the plasma chamber. Given the absence of C-F bonds in the C1s peak, this negligible contamination will not affect the triboelectric properties of the wood sample. Even though the O_2 plasma treatment changes the ratio of functional groups on the wood surface, it does not introduce any new chemical functionality with strong ability to gain or lose electrons. As such, the contribution of O_2 plasma treatment to the improvement of wood's triboelectrical properties should mainly arise from the morphological, rather than the chemical, changes produced.

Conversely, wood treated with the $C_4F_8 + O_2$ plasma displays a strong fluorine peak, as shown in Fig. 3e. Compared to native wood, the oxygen concentration is reduced to 3.6%. The peak deconvolution of C1s spectrum was made assuming carbon to be bonded only to fluorine or CF_x species (Fig. 3f). Compared to native wood, the amount of C–C bonds was also reduced (30.6%) and three new peaks appeared, associated to C-CF (21.3%), CF (21.5%), CF_2 (18.3%) and CF_3 (8.3%) [36]. In addition, the amount of fluorine grafted on wood surface increases from 42.9% to 51.4% when the exposure time is increased from 5 min to 15 min, as shown in Fig. S5. The XPS results indicate that, unlike O_2 plasma, the $C_4F_8 + O_2$ plasma treatment results in a dramatic chemical modification of the wood surface. Given the very high electron affinity of fluorine, we expect wood fluorination to significantly enhance its ability to acquire electrons, consequently increasing the W-TENG performance.

The working mechanism of a TENG is based on the coupled effects of contact electrification and electrostatic induction. The process of contact electrification involves the mechanical friction of two materials and the consequent generation of charges with opposite signs on their respective surfaces [44]. An electron cloud/potential well model at the atomic scale was proposed recently to explain contact electrification between solid–solid pairs in which electrons do not have individual energy levels

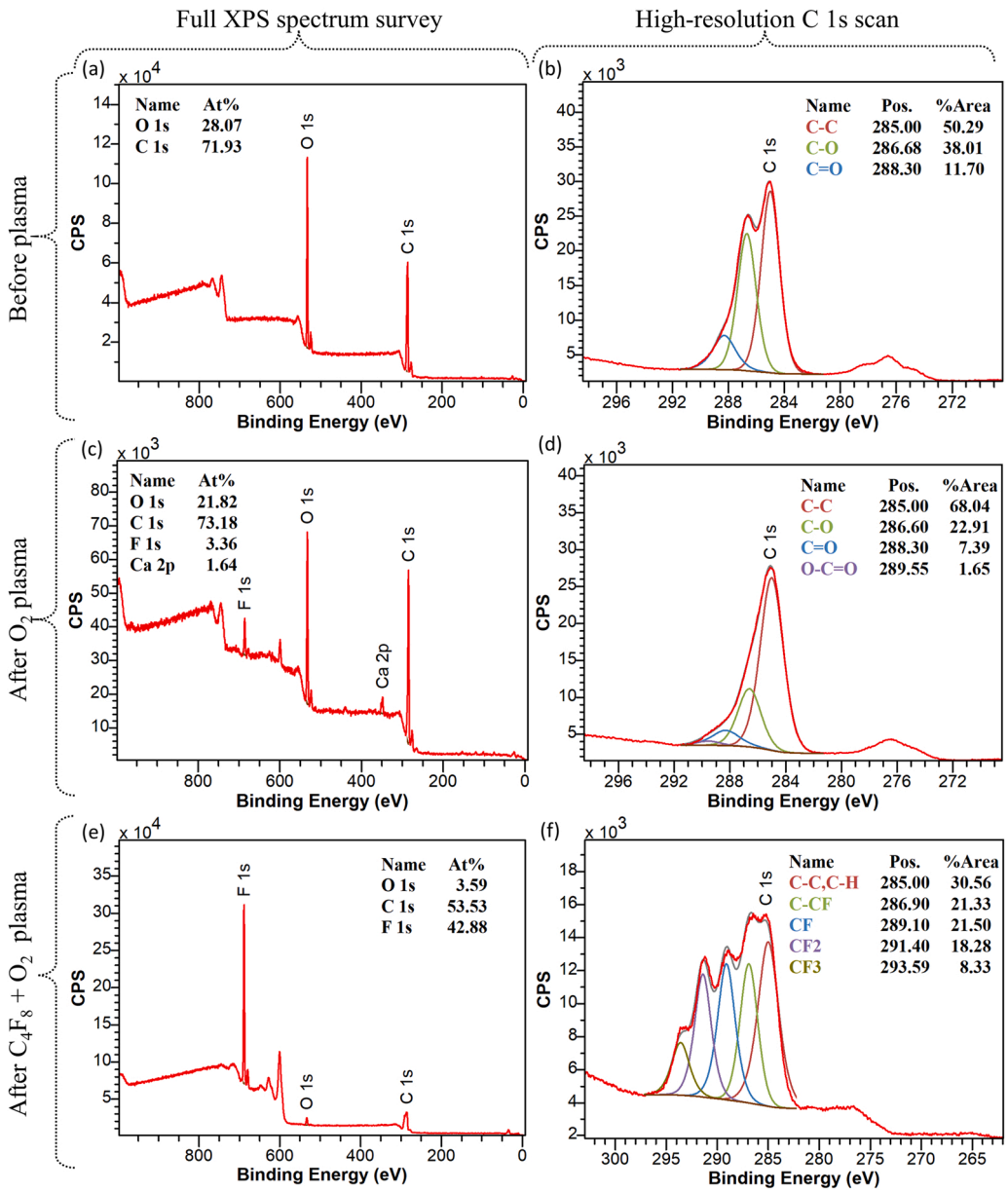

Fig. 3. Surface chemistry of native wood and plasma-treated wood. (a) Full XPS spectrum survey for radial-cut native wood. (b) High-resolution C 1 s scan for radial-cut native wood. (c) Full XPS spectrum survey for radial-cut O_2 plasma-treated wood. (d) High-resolution C 1 s scan for radial-cut O_2 plasma-treated wood. (e) Full XPS spectrum survey for radial-cut $C_4F_8 + O_2$ plasma-treated wood. (f) High-resolution C 1 s scan for radial-cut $C_4F_8 + O_2$ plasma-treated wood.

(*e.g.* the wood-wood pair in the present study) [45],[46]. As illustrated in Fig. 4a, an atom in modified wood can be represented by a potential well, where the outer shell electrons are loosely bound, forming an electron cloud (*i.e.* electrons that are spatially localized to specific atoms or molecular orbitals) [44]. Before atomic-scale contact, the electron clouds in two modified wood surfaces are separated without overlap and the electrons are tightly confined in their original orbits by the potential wells with a high escaping energy barrier. When atoms from each surface get close enough and contact each other their electron clouds strongly overlap, and the single potential wells become asymmetric double-wells. As a result, electrons with higher energy from a modified wood surface can easily overcome the reduced interatomic potential barrier and be transferred to an atom in the other modified wood surface. As illustrated in Fig. S6, a subsequent electrostatic induction process is needed to harvest the charges generated by contact electrification. Initially, because the opposite charges generated by contact electrification are fully balanced, there is no electron flow in the external circuit [17]. When the two materials are separated, most of the transferred electrons remain as surface static charges due to the high energy barrier. However, these charges with opposite signs cannot be compensated by each other, generating a potential difference across two electrodes. Opposite charges are induced on the back electrodes under the effect of electrostatic induction, driving the current flowing in the external circuit in order to screen the potential difference [47]. This transient flow of current continues until the two modified wood surfaces are fully separated. Once the contact is reversed, the electrons will flow back in the opposite direction until the initial state is obtained, leading to a reversed electrical output.

Based on the above-described mechanism, the triboelectric performance of different plasma-treated wood samples were systematically investigated, and the results summarized in Fig. 4b-g. Wood treated with O_2 plasma and with $C_4F_8 + O_2$ plasma were separately assembled in a TENG against a radial-cut native wood in a simple vertical contact-separation TENG design. First, O_2 plasma treatment was applied to

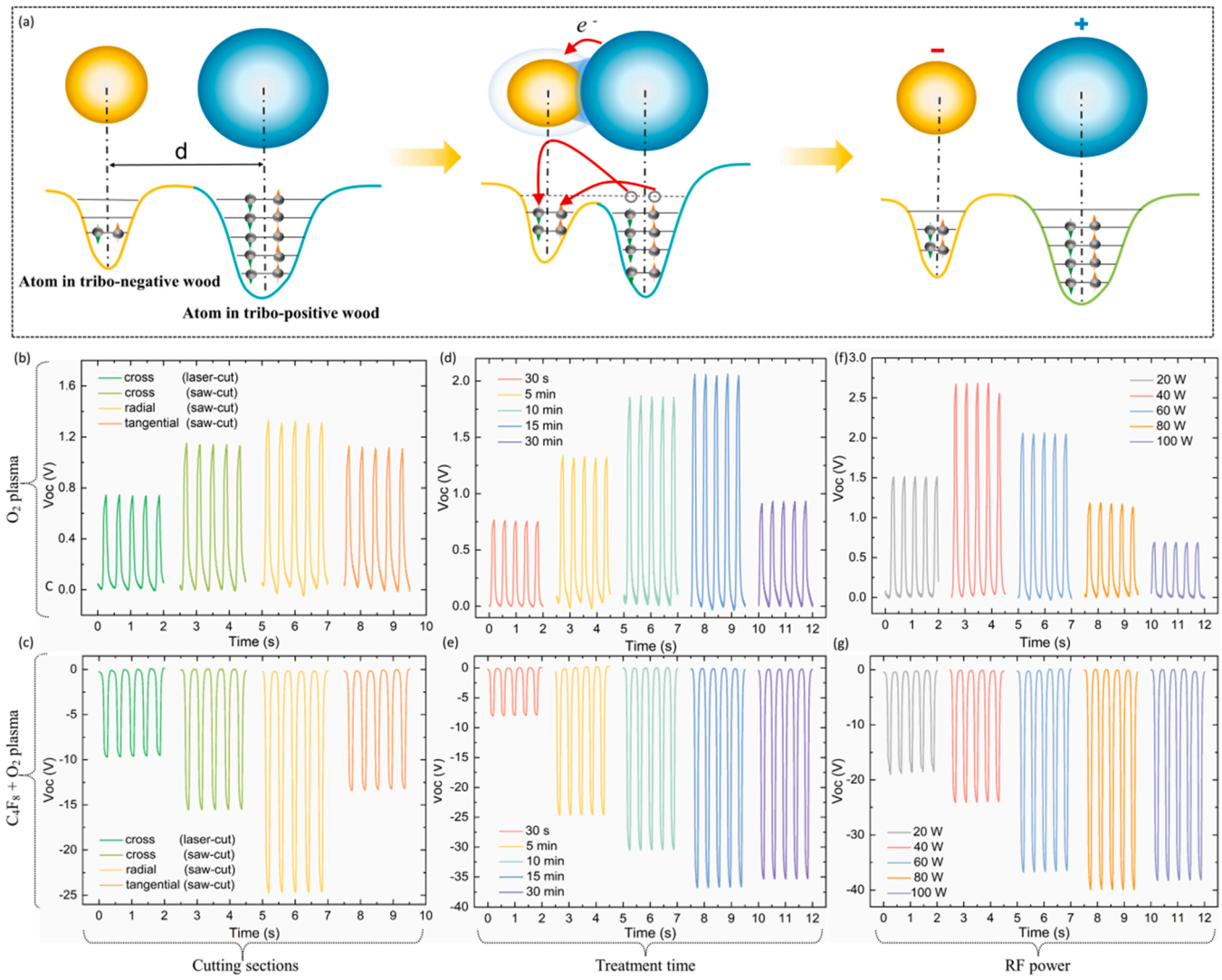

Fig. 4. In-depth working mechanism and triboelectric performance of wood TENGs. (a) Schematic representation of the atomic-scale electron cloud/potential well model used to describe the contact electrification process of a wood-TENG. (b) Open-circuit voltage of W-TENG composed of a piece of radial-cut native wood against a piece of O_2 plasma-treated wood cut in different sections. The power and time of plasma treatment are 60 W and 5 min, respectively. (c) Open-circuit voltage of W-TENG composed of a piece of radial-cut native wood against a piece of $C_4F_8 + O_2$ plasma-treated wood cut in different sections. The power and time of plasma treatment are 60 W and 5 min, respectively. (d) Open-circuit voltage of W-TENG composed of a piece of radial-cut native wood against a piece of radial-cut wood treated with O_2 plasma with 60 W power for various exposure times. (e) Open-circuit voltage of W-TENG composed of a piece of radial-cut native wood against a piece of radial-cut wood treated with $C_4F_8 + O_2$ plasma with 60 W power for different exposure times. (f) Open-circuit voltage of W-TENG composed of a piece of radial-cut native wood against a piece of radial-cut wood treated with O_2 plasma for 15 min with various power values. (g) Open-circuit voltage of W-TENG composed of a piece of radial-cut native wood against a piece of radial-cut wood treated with $C_4F_8 + O_2$ plasma for 15 min with various power values.

wood veneers cut in different directions and with different techniques, namely: cross-cut veneer (cut by laser), cross-cut veneer (cut by saw), radial-cut veneer (cut by saw), and tangential-cut veneer (cut by saw). The power and time of plasma treatment were fixed at 60 W and 5 min, respectively. Then, these O_2 plasma-treated wood samples were paired with a radial-cut native wood veneer. The electrical performance of each wood-TENG is illustrated in Fig. 4b and Fig. S7. The surface area for the devices in Fig. 4 is kept constant at 2 cm × 3.5 cm, in 1 mm thickness, and the applied force is always 40 N. It can be seen that, when paired with radial-cut native wood, the O_2 plasma-treated cross-cut wood (cut by laser) tends to generate a lower electrical output than cross-cut wood (cut by saw). This result may be attributed to the highly porous structure of the cross-section, in which the big and deep pores may reduce the effective contact surface area. The remaining three wood samples have a similar microscale roughness, with only small differences arising from their characteristic textures, and, after the O_2 plasma treatment, they tend to generate a similar electrical output. The best performance is given by radial-cut wood, with a voltage of 1.33 V and a current of 0.024 μA. As a control experiment, we paired together two pieces of native radial-cut wood and measured the triboelectric output. As shown in Fig. S8, this native wood-TENG produced much lower voltage and current, respectively 0.254 V and 0.0038 μA. This scarce output can be attributed to the inherently poor polarizability of wood and the weak triboelectrification effect between two identical materials. It is clear from these results that the O_2 plasma treatment does increase the electrical performance of wood, but with an increment of only about five times.

Conversely, significant changes in the triboelectric behavior of wood were observed by applying the $C_4F_8 + O_2$ plasma treatment to the four different kinds of wood samples, all the other parameters being the same. As shown in Fig. 4c, the output voltage of the $C_4F_8 + O_2$ plasma-treated wood has a reversed polarity compared to the O_2 plasma-treated ones (from more positive to more negative values). This indicates that the triboelectric behavior of plasma-treated wood can be changed from

electron-donating to electron-accepting depending on the composition of the plasma. Furthermore, the output voltages generated from the mixed plasma wood-TENGs are much higher than those generated by O_2 plasma-treated TENGs, with the highest voltage of 24.7 V contributed by plasma-treated radial-cut wood. Compared to the W-TENG composed of two pieces of native wood, the electrical output after the $C_4F_8 + O_2$ plasma treatment is increased by almost a hundred times. This huge difference compared to the five times improvement observed for the O_2 plasma-treated wood could be explained by taking into account that, as previously discussed, the wood surface modifications produced by the O_2 plasma treatment are mostly of physical nature, while the $C_4F_8 + O_2$ plasma modifies the surface chemical composition, introducing species with strong electron-accepting ability.

We showed already that both the surface roughness and chemical composition of a wood surface can be affected not only by the composition of plasma but also by other parameters, such as treatment time. In the following, we studied the effect of different treatment times (ranging from 30 s to 30 min) on the electrical performance of W-TENGs while keeping all other conditions (chemical composition, 60 W power, 5 Pa working pressure) constant. For this investigation, we will focus on radial-cut wood, since it shows the best performance and is most suitable for large-scale fabrication. As shown in Fig. 4d and Fig. S9, both the voltage and current output of O_2 plasma-treated samples gradually increase for exposure times increasing up to 15 min, thanks to the enhanced surface roughness. However, when the exposure time is further increased to 30 min, the voltage drops to 0.93 V, from the peak value of 2.06 V. This abrupt decrease may be due to the surface damage generated by prolonged etching. As shown in Fig. S10, under these treatment conditions many surface layers of wood cells were completely removed, exposing the underlying layer and leading to an excessively rough surface, thus reducing the positive contribution of the generated nanostructures. Similarly, the electrical output of $C_4F_8 + O_2$ plasma-treated samples increases as a function of the exposure time up to 15 min, as shown in Fig. 4e and Fig. S9. The improved performance is related to the increased amount of fluorine grafted to the wood surface. Unlike the O_2 plasma-treated wood, extending the treatment time to

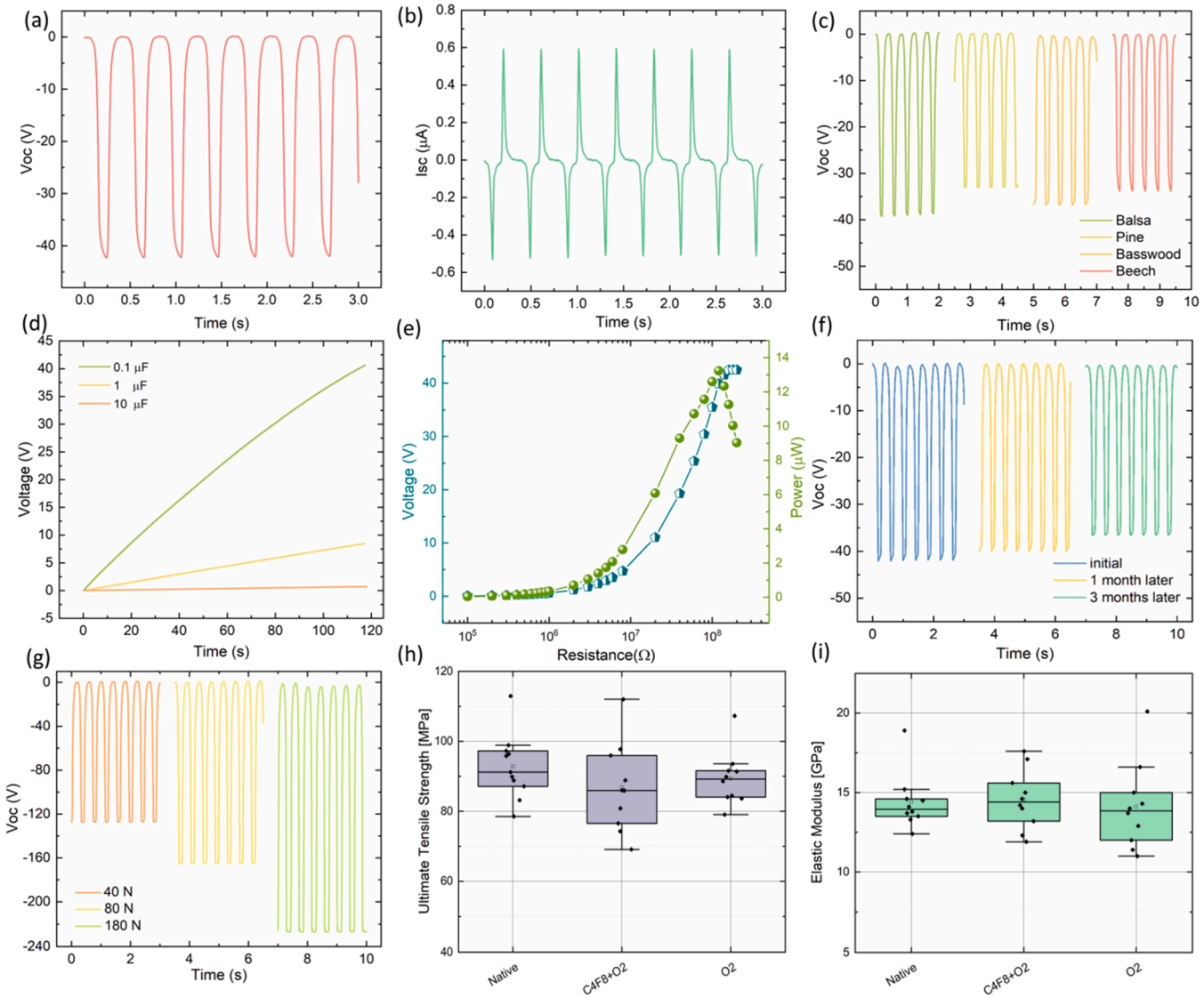

Fig. 5. Electrical output and other properties of the optimized W-TENG. (a) Open-circuit voltage and (b) short circuit current of a W-TENG made of two pieces of radial-cut plasma-treated wood. The treatment conditions were, respectively: 15 min, 80 W power for the $C_4F_8 + O_2$ plasma, and 15 min, 40 W power for the O_2 plasma. (c) Open-circuit voltage of W-TENG made from different wood species. (d) Voltage profile of capacitors (0.1 μF, 1 μF, 10 μF) when charged by the plasma-treated W-TENG. (e) Electrical output performance of the plasma-treated W-TENG with an external loading resistance. (f) Stability test for up to 3 months. (g) Open-circuit voltage of the larger-sized plasma-treated W-TENG (10 cm × 8 cm) under different forces. (h) Ultimate tensile strength and (i) stiffness values of native spruce (R), and wood samples treated with O_2 plasma (40 W, 15 min) and with $C_4F_8 + O_2$ plasma (80 W, 15 min), respectively.

30 min results in a slight decrease of the voltage output, from 36.7 V to 35.4 V. The associated current shows a similar trend. This different behavior compared to O_2 plasma-treated wood may result from the non-etching effect of the $C_4F_8 + O_2$ plasma. The XPS spectrum in Fig. S11 indicates that the amount of fluorine atoms on the wood surface after a 30 min-treatment is similar to that measured after 15 min, probably due to the saturation of the surface with fluorine atoms. Based on these results, we consider 15 min to be the best treatment time for both the O_2 and $C_4F_8 + O_2$ plasmas.

Then, we performed a similar study to determine the effect of the plasma treatment power, in a range from 20 W to 100 W. As shown in Fig. 4f and Fig. S12, the maximum electrical output (~2.67 V and 0.041 μA) for the O_2 plasma-treated TENG is obtained, with a power of 40 W. The output decreases with further increase in power. Compared to the output of a W-TENG made with a pair of native wood samples, the O_2 plasma treatment can improve the electrical output of wood by 10 times. The maximum electrical output (~39.8 V and 0.46 μA) for the $C_4F_8 + O_2$ plasma-treated wood is obtained for a power of 80 W, and decreases slightly when the power is further increased to 100 W (see Fig. 4g and Fig. S12). Hence, with the $C_4F_8 + O_2$ plasma treatment it is possible to increase 156 times the electron-attractive ability of wood.

Our results demonstrate that the triboelectric polarity of wood can be properly enhanced and tuned using different plasma treatments (Fig. S13). Wood can be enabled with a broader spectrum of triboelectric behaviors, more tribopositive (O_2 plasma) as well as more tribonegative ($C_4F_8 + O_2$ plasma). The electrical output of a W-TENG made with a pair of 2 cm × 3.5 cm radial-cut wood samples (one treated with O_2 and the other with $C_4F_8 + O_2$ plasma), can be more than 166 times higher than that of native wood, with an open-circuit voltage and short current of, respectively, 42.3 V and 0.6 μA (Fig. 5a, b).

The influence of wood species was also investigated. Besides spruce, the plasma treatments were also applied to four different wood species, including softwood (pine) and hardwood (balsa, basswood and beech), using the conditions optimized for spruce (40 W, 15 min for the O_2 plasma; 80 W, 15 min for the $C_4F_8 + O_2$ plasma). The results are shown in Fig. 5c. Under the same testing conditions, pine, basswood, balsa and beech could generate a voltage similar to that of spruce, respectively 32.9 V, 36.7 V, 39.3 V and 33.8 V, suggesting the universality of plasma treatment for enhancing the triboelectric performance of wood. It is reasonable to hypothesize that different kinds of wood would require dedicated parameter optimization. Nevertheless, the electricity produced by a plasma-treated spruce W-TENG is sufficient to power small electronic devices and can be efficiently stored in a capacitor. As shown in Fig. 5d, commercial capacitors with three different capacities (0.1 μF, 1 μF, and 10 μF) were charged using the spruce W-TENG developed here. In 118 s, the 0.1 μF capacitor could reach 40.6 V, the 1 μF capacitor could reach 8.5 V, while the 10 μF capacitor could only reach 0.7 V. To further evaluate the resistance-dependent performance of our plasma-treated W-TENG, external resistances varying from 0.1 to 200 MΩ were connected. As shown in Fig. 5e, the instantaneous voltage value gradually increases as a function of increased resistance, and then tends to plateau. The instantaneous power reached a maximum value of 13.2 μW, corresponding to a power density of 18.86 mW/m^2 with an optimized load resistance of 120 MΩ.

Stability plays a fundamental role in determining real-world applications of TENGs. Aging, that is deterioration of desired properties, is a common issue of plasma-modified surfaces. Aging can happen due to various processes that happen after the plasma treatment, such as the diffusion or reorientation of surface functional groups, and especially environmental contamination. Thus, besides treatment parameters (*e.g.* gas, treatment time, and power), the stability of the plasma-induced surfaces strongly depends on their storage conditions. For this reason, we prepared two pairs of plasma-treated W-TENGs to test their stability and durability for up to 3 months under two different environmental conditions. The first pair of W-TENGs was left completely exposed to air, and their output showed a sharp decrease (> 50%) after one month (Fig. S14). Then, the output seemed to stabilize, with only a slight decrease after an additional two-months exposure. The other pair of W-TENG was kept in a sealed bag, and it showed good stability even after 3 months, as shown in Fig. 5f. Thus, the aging of plasma-treated wood is more pronounced when the samples are continuously exposed to the atmosphere, while it can be effectively reduced by sealing them in a transparent polyethylene bag. In addition, we investigated the electrical output of the W-TENG for different relative humidity (RH) conditions and found that RH of 30%− 50% shows limited impact while humidity higher than 60% or even 70% shows obvious negative impact on the W-TENG output (Fig. S15). For real-world applications, we envisage our W-TENG as the active part of a self-powered wooden floor. In such a configuration, the W-TENG would be sealed and protected from the surrounding environment, thus ensuring a relatively stable and durable electrical output.

Scalability also plays a vital role for smart building applications. To demonstrate it, we increased the size of plasma-treated wood samples to 10 cm × 8 cm. As shown in Fig. 5g and Fig. S16, the larger-sized W-TENG can generate a higher voltage and current of 127.2 V and 1.4 μA respectively, under a force of 40 N. Higher forces will induce higher electrical outputs. Accordingly, increasing the force to 180 N resulted in an electrical output of 227 V and 4.8 μA demonstrating the feasibility of large-scale practical applications *e.g.* as energy-generating floorings.

Mechanical strength is of great importance for materials to be used in building applications. For this reason, the plasma-treated wood samples were also characterized by tensile tests (Fig. 5h and i). The ultimate tensile strengths of spruce treated with O_2 plasma (40 W, 15 min) and with $C_4F_8 + O_2$ plasma (80 W, 15 min) were, respectively, 88.6 MPa and 85.9 MPa, only slightly lower than that of native spruce(R) (91.2 MPa). The stiffness (Fig. 5h) of spruce treated with O_2 plasma (40 W, 15 min) and treated with $C_4F_8 + O_2$ plasma (80 W, 15 min) was, respectively, 13.8 GPa and 14.4 GPa, comparable to that of native spruce(R) (13.9 GPa). These results indicate that the tensile stiffness and strength of wood are well-preserved by the plasma treatment. Last but not least, the natural wood surface color is preserved too, as can be seen from Fig. S17 and the small color change (ΔE*) values listed in Table S3. This is especially important for indoor building applications, given the potential psychological benefits to humans deriving from the warm colors of wood [48].

It is noteworthy to highlight here that, since our primary intention was to improve the electrical output of wood-TENGs while adhering to realistic use scenarios in buildings, we used wood veneers of much higher thickness compared to that of other triboelectric materials [8]. This helps ensuring sufficient mechanical robustness but at the same time weakens the electrostatic induction effect. For this reason, the electrical output of our plasma-treated wood-TENG is not superior to that of state-of-art wood- or cellulose-based TENGs (Table S4) [8,49,50]. Nevertheless, at the end of TENG's service life these materials can be very easily separated from wood for proper disposal and recycling: the metal electrodes can be peeled off and the fluoropolymer sliced away revealing the intact bulk wood. A dedicated life-cycle analysis is beyond the scope of the present work, but could help ascertain the true potential of our wood-TENGs by correlating performance efficiency, low material and manufacturing costs, and a favorable environmental profile[51,52].

To showcase the suitability of our plasma-treated wood for large-scale applications, we discuss here the fabrication and working operation of two prototypes of triboelectric wood floorings, with double- or single-electrode configuration.

Fig. 6a illustrates the typical configuration of a self-powered floor demonstrator, made of many pairs of large-sized plasma-treated wood-TENGs connected together. In this configuration, springs are used to create a variable gap between the O_2 plasma- and of $C_4F_8 + O_2$ plasma-treated wood veneers, enabling to trigger triboelectrification in contact-separation mode when walked upon. Such a floor could generate enough electricity to power directly energy-intensive devices such as lamps. In addition, the electricity produced in excess could be stored for later use,

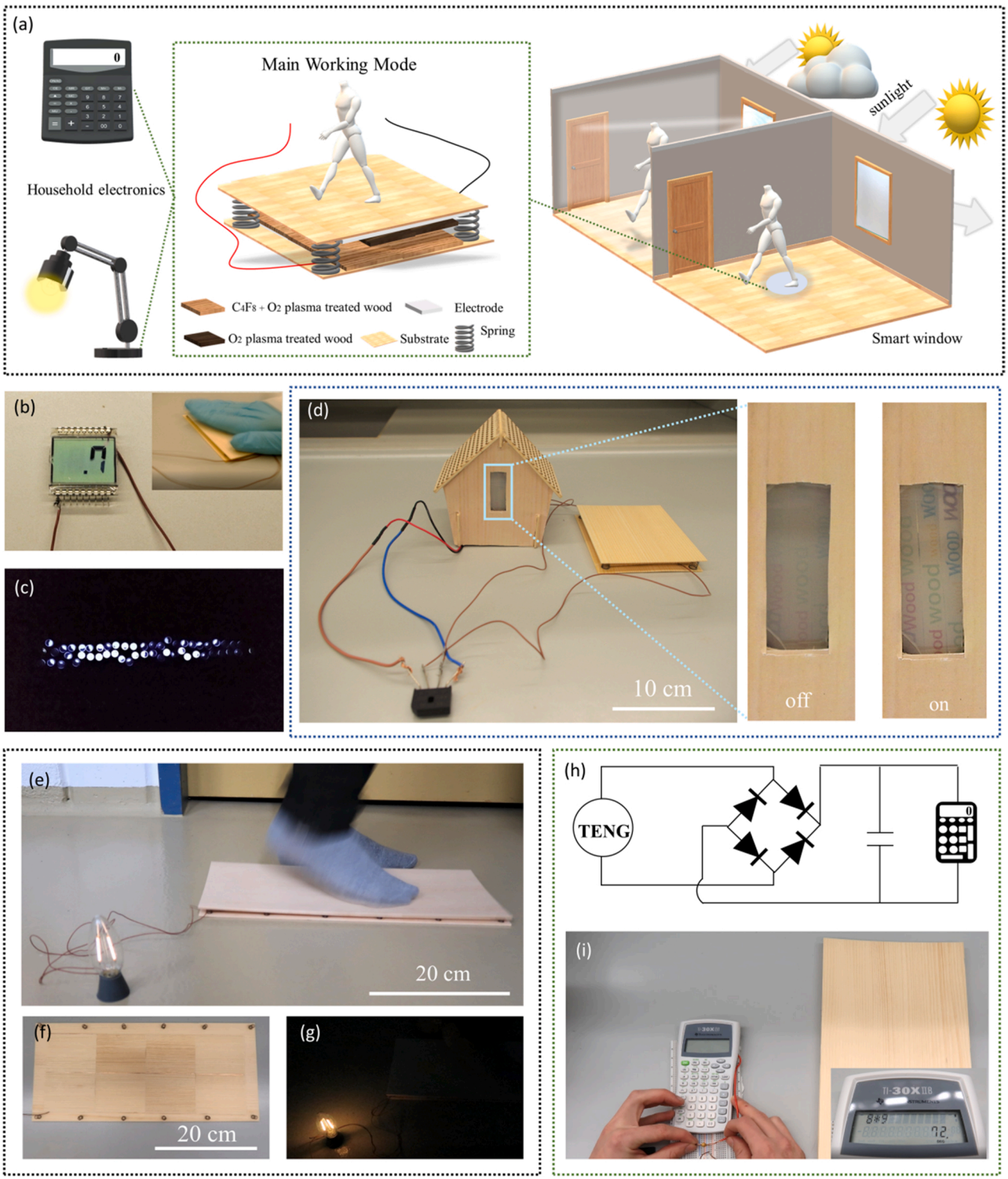

Fig. 6. Main configuration of self-powered wooden floor and its practical applications. (a) Schematic representation of a W-TENG floor with main configuration and its applications in smart buildings to power household electronics and smart windows. (b-d) A W-TENG floor made of one pair of 10 cm × 8 cm O_2 plasma- and C_4F_8 + O_2 plasma-treated wood veneer was used to power a LCD screen, an array of 52 LEDs, and the smart window of a model wooden house, respectively. (e-g) A bigger prototype (45 cm × 20 cm) of W-TENG floor made of eight pairs of plasma-treated wood connected was used to power a household lamp (2 W, E14). (h-i) A bigger prototype (45 cm × 20 cm) of W-TENG floor made of eight pairs of plasma-treated wood connected was used to charge a capacitor and then power a calculator.

contributing to the reduction of the energetic demand of the building.

Fig. S18 displays a prototype of a self-powered wooden floor composed of one pair of 10 cm × 8 cm-sized O_2 plasma- and of C_4F_8 + O_2 plasma-treated wood veneers. Copper foils are attached to the backside of the plasma-treated veneers as electrodes, and can be easily peeled off at the end of service life for proper disposal and recycling. Finally, two pieces of wood veneers (10 cm × 8 cm × 0.3 cm) are used to cover the electrode and serve as substrate, while springs at the corners act as spacers. As shown in Fig. S19, the floor prototype could be connected directly to an array of commercial light-emitting diodes (LEDs) or

to a liquid crystal display (LCD) without the need for a storage or power management unit. As shown in Fig. 6b, 6c and in the Video S1 and S2, fifty-two LEDs and a LCD can be powered by pressing the W-TENG with one hand. To demonstrate its application to power smart windows, the wooden floor was connected to a full-wave bridge rectifier, which was then connected to the smart window of a small model house. As shown in Fig. 6d, Fig. S20, and in the Video S3, the window is opaque, but becomes transparent when the wooden floor is pressed by hand.

To further demonstrate the upscaling potential for integration in smart buildings, we fabricated a bigger prototype of a triboelectric wooden floor with eight plasma-treated W-TENGs electrically connected together. Copper foils (40 cm × 16 cm) were attached to the back of the W-TENGs and covered with a larger native wood veneer (45 cm × 20 cm × 0.3 cm). Conductive wires were led out from the electrodes and directly connected to a big household lamp (2 W, E14). As shown in Fig. 6e-g and Video S4, the household lamp can be readily switched on, emitting a relatively strong light in both bright and dark environments, when the triboelectric wood floor prototype is walked upon. Since we have demonstrated that the electricity produced by a W-TENG could be stored in a capacitor, a circuit integrating the W-TENG floor with a full-wave bridge rectifier, with a 47 μF capacitor, was designed to generate the stable DC output necessary for powering a commercial calculator, as depicted in Fig. 6h. After pressing on the demonstrator for a few seconds, both a low-power and a high-power calculator could be powered stably (see Fig. 6i, Fig. S21, Video S5).

Although powerful, the triboelectric wood flooring in contact-separation mode suffers from an important inconvenience, that is, the associated bending could affect the balance of people walking on it. This issue can be conveniently addressed by an alternative design: a self-powered floor with a single-electrode configuration. The device has only one electrode and one triboelectric layer, while an external object (*e.g.* shoe soles, socks, human skin, and so on) serves as the counter triboelectric layer. As illustrated in Fig. 7a, either O_2 plasma- or $C_4F_8 + O_2$ plasma-treated wood veneers could serve as the only triboelectric layer, with a copper foil attached on the back as the conductive electrode, which is also connected to the ground by a metal wire through an external load.

Fig. 7b schematically depicts the working principle of this single-electrode W-TENG. When external objects contact the surface of plasma-treated wood, charges with different polarities are generated on their respective surfaces due to contact electrification. Electrons are injected from the tribopositive surface to the tribonegative one, resulting in fully balanced charges. Hence, there is no electron flow in the external circuit at this stage. Once the external object is separated from the wood surface, the charges on its surface are not compensated anymore and the electrostatic equilibrium is broken. Subsequently, charges of opposite signs are induced on the copper electrode, driving the flow of electrons from the copper electrode to the ground *via* the external load. This process continues until the charges on the wood surface are fully screened. When the external object approaches the wood surface again, the electrons flow back in the opposite direction until the original state is attained [17].

Based on the described working principle, the electrical output of this one-electrode W-TENG heavily relies on the differences in polarity

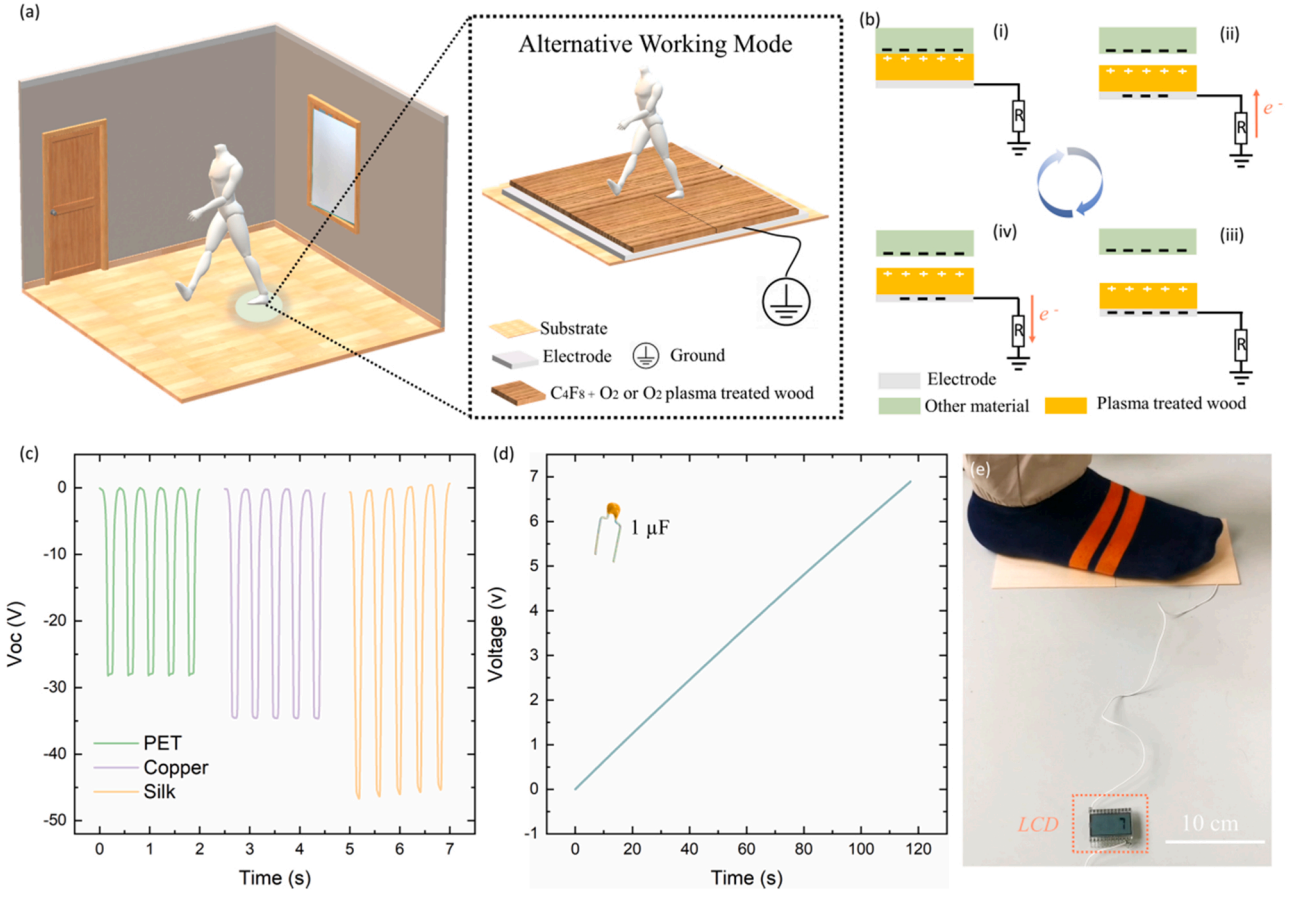

Fig. 7. Single-electrode configuration of self-powered wooden floor and its practical applications. (a) Schematic representation of a W-TENG floor with single-electrode configuration. (b) Schematic representation of operation principle for the single-electrode W-TENG. (c) Output voltage of $C_4F_8 + O_2$ plasma treated single-electrode W-TENG when contacting with different materials. (d) Voltage profile of a capacitor (1 μF) when charged by the $C_4F_8 + O_2$ plasma treated single-electrode W-TENG when contacting copper foil. (e) A single-electrode W-TENG floor made of 2 pieces of 12 cm × 10 cm $C_4F_8 + O_2$ plasma-treated wood veneer was used to power a LCD screen.

between plasma-treated wood and external objects. To demonstrate it, we fabricated a 2 cm × 3.5 cm single-electrode W-TENG with a piece of radial-cut wood (80 W, 15 min for the $C_4F_8 + O_2$ plasma). Then, we contacted it with poly(ethylene terephthalate) (PET, a plastic commonly used for textiles), copper foil and silk, respectively. Under a force of 40 N, the corresponding open-circuit voltages were, respectively, 27.9 V, 34.6 V and 46.2 V (Fig. 7c). Also, the electricity produced by the single-electrode W-TENG can be stored in a capacitor. As shown in Fig. 7d, a commercial 1 μF capacitor was successfully charged in 118 s to 6.9 V by contacting this single-electrode W-TENG with copper foil. To demonstrate the scalability of this single-electrode W-TENG, we increased its size to 12 cm × 10 cm. As shown in Fig. S22, the larger-sized single-electrode W-TENG can generate a voltage of 205.9 V under a force of 180 N when contacted with a copper foil of the same size. To demonstrate the upscaling potential for smart building applications, we fabricated a relatively bigger prototype, which could accommodate a foot, with two pieces of $C_4F_8 + O_2$ plasma treated wood. Copper foil with a size of 24 cm × 10 cm was attached to the back of this single-electrode W-TENGs, connected to a LCD and to the ground, as shown in Fig. S23. As shown in Fig. 7e, Fig. S24 and Video S6, the LCD could be easily switched on when the prototype was pressed either by a human foot wearing a sock or a naked hand.

Compared to the previously described contact-separation working mode, this single-electrode design is cheaper, as it needs only one triboelectric layer and one electrode, and more practical as it avoids floor deformations. However, the direct contact with external objects (*e.g.* dirty soles) may result in a quickly deterioration of the triboelectric surface, reducing its durability. Moreover, compared to the contact-separation mode W-TENG, its electrical output is completely dependent on the triboelectric polarity of the external objects with which it is contacted.

Both configurations, contact-separation and single-electrode, have complementary advantages and disadvantages. More research is needed to find better solutions. In the present study, we wanted to demonstrate the great potential of triboelectric wood for real-world applications. Based on our results, we can already envision large-scaled wood floorings that would allow to power a variety of electronic devices, generating electricity from human activities as common as walking, thus partially reducing the reliance of smart buildings on the public electricity network.

3. Conclusion

We demonstrated how to enhance to a great extent the otherwise negligible triboelectric behavior of native wood using the consolidated and scalable technology of plasma treatments. Our approach offers great promises to help mitigate the economic and environmental challenges posed by the large-scale fabrication of high-performance TENGs that so far have hindered their successful adoption in smart buildings. We have explored in detail the interplay between wood and plasma treatment parameters, and the impact on the final triboelectric properties of wood. With optimized parameters, O_2 plasma-treated wood can be made up to 10 times more tribopositive than native wood, while when treated with a $C_4F_8 + O_2$ plasma wood becomes 156 times more tribonegative. These dramatic changes of tribopolarity are attributed to different mechanisms, respectively of physical (nanostructuration and consequent increase of surface roughness produced by the etching action of O_2 plasma on wood) and chemical nature (modification of wood surface composition by grafting efficient electron-acceptor fluorinated species). When two wood samples (20 × 35 × 1 mm^3), one treated with O_2 plasma and the other with $C_4F_8 + O_2$ plasma, are placed in contact with a force as low as 40 N, a maximum voltage of 42.3 V and a current of 0.6 μA are generated. The output voltage can be further increased by an order of magnitude by increasing the size of the W-TENG, demonstrating its scalability in both size and performance. Our wood floor prototype with W-TENGs, made of several pairs of large-size plasma-treated wood, could be used to power directly a variety of electronic appliances or to store the produced electricity produced in capacitors for later use. To avoid the problem of floor deflection and bending during the operation of the contact-separation mode W-TENG, we propose an alternative design of self-powered floor with a single-electrode configuration. These results provide useful insight into the physics behind tuning the tribopolarity of wood with an added value in terms of preservation of wood's intrinsic properties. Our work is a step towards the development of next-generation large-scale self-powered building materials, opening up favorable technological pathways towards a 'net-zero emissions' future by contributing to the decarbonization of the built environment.

4. Experimental section

4.1. Plasma treatments

Plasma treatments were performed in a home-built capacitively coupled plasma reactor driven by 13.56 MHz radio frequency (RF) excitation as described in more detail elsewhere [53]. Wood samples were placed on the bottom RF electrode (10 ×15 cm^2). Etching with an O_2 plasma was carried out at a working pressure of 5 Pa and oxygen flow rate of 20 standard cubic centimeters per minute (sccm). Plasma treatment with a mixture of O_2 (2 sccm) and C_4F_8 (18 sccm) was conducted at the same working pressure. The applied RF power and time can vary from 20 W to 100 W and 30 s to 30 min, respectively. After the treatment, the reactor system was vented with nitrogen gas and the samples were removed from the reactor.

4.2. Scanning electron microscopy (SEM)

Wood samples were cut into small cubes of 10 mm × 10 mm × 1 mm. Then, they were dried in a vacuum oven at 103 ℃ for 2 h. Afterward, the wood samples were coated with Pt–Pd (80/20) film to make their surface electrically conductive. A sputter-coater (CCU-010, Safematic, Switzerland) was used, adjusting the thickness of the coating to about 10 nm. The structure of the samples was characterized by field emission scanning electron microscopy (FEI Quanta 200 F).

4.3. Atomic force microscopy (AFM)

AFM imaging was performed at 20 °C and 65% relative humidity on a NanoWizard 4 (JPK Instruments AG - Bruker Nano GmbH, Germany). The samples were fixed to SEM sample mounting stubs using carbon tabs, with the radial-longitudinal surface oriented parallel to the stub surface. Measurements were performed in alternating contact mode (AC mode), using pyramid-shaped silicon cantilevers (NCHR-10, Nano World, Switzerland) with a resonant frequency of 320 kHz and a nominal spring constant of 42 N m^{-1}. A scan size of 2.5 × 2.5 μm and a resolution of 256 × 256 pixels were used. Imaging was performed at scanning rates of 0.3–0.5 Hz and setpoint amplitudes of 65–75% of the free oscillation amplitude. All images were first analyzed with the JPK image processing software (JPK Instruments AG - Bruker Nano GmbH, Germany), where a background tilt correction and a basic line correction were applied. Outliers and scars were replaced by applying the median of neighboring pixels and neighboring lines, respectively. Finally, all images were plotted using the Gwyddion software (v 2.5).

4.4. Surface profilometry

Surfaces were profiled with a Bruker Dektak XT Stylus profilometer (Bruker Corporation, Billerica, MA) equipped with a 2 μm radius tip.

4.5. X-ray photoelectron spectroscopy (XPS)

XPS Spectra were obtained with a SPECSTM spectrometer (SPECS GmbH, Germany) using a Mg Kα X-ray source (λ = 1253.6 eV) with a

power of 300 W. The measurements were performed at room temperature. Each sample was measured at three spots. The investigated area was typically 1 × 3 mm^2. Survey spectra were acquired over a binding energy range of 0–1000 eV at pass energy of 30 eV and resolution of 0.5 eV/step. High-resolution spectra of C 1 s, and O 1 s were an average of three scans acquired at a pass energy of 20 eV and resolution of 0.05 eV/step. The spectra were collected in the same order for each sample (survey, C 1 s, O 1 s). The CasaXPS software was used for background subtraction (U2 Tougaard-type), peak integration, quantitative chemical analysis and deconvolution. The C 1 s (C–C) peak at 285 eV was used to calibrate the binding energy scale.

4.6. Electrical measurements

A linear motor (PL01–28 ×500/420) was used to load the samples with a fixed force. At the same time, a loading cell was mounted on the rigid frame of the motor to monitor the pressure applied on the samples. Finally, the electrical output was measured by Keithley 6514 equipped with Matlab software. The controlled experiments were performed at 25 ℃ with 30% humidity.

4.7. Measurement of color changes

Changes in color of wood surface were measured with a Minolta spectrophotometer (CR200, Japan) using the CIE L*a*b* system based on the ISO 7724 standard test method [54]. The average values of the color parameters were obtained by measuring ten different positions for each sample. In the CIE L*a*b* system, L represents lightness, a and b represent chromaticity parameter. The overall color change (ΔE*) was calculated according to the following equation (Eq. 1):

$$\Delta E^{*} = \sqrt{\Delta a^2 + \Delta b^2 + \Delta L^2} \quad (1)$$

where ΔL, Δa, and Δb represent the changes in L, a, and b between the values of native wood and plasma treated wood, respectively. A lower ΔE* value corresponds to a lower color change.

4.8. Mechanical tensile testing

Tensile tests were conducted on a Zwick/Roell Z010 universal testing machine, using a 10 kN load cell. The samples were cut into dog bone shape according to ISO 527–3 [21]specimen type 5 parallel to the fiber direction. Then, spruce tags were glued to the grip section of the samples as reinforcement. The displacement was measured in the narrow parallel-sided portion of the sample using a clip-on extensometer. During testing, the speed was 0.4 mm/min. The Young's modulus E was calculated from the stress-strain curve as the slope of a linear regression in the range between 10% and 40% of the maximal force.

CRediT authorship contribution statement

Jianguo Sun: Conceptualization, Methodology, Resources, Formal analysis, Data Curation, Writing – original draft, Writing – review & editing, Visualization, Supervision **Urs Schütz:** Methodology, Resources, Data curation, Supervision. **Kunkun Tu:** Methodology, Writing – review & editing. **Sophie Marie Koch:** Methodology, Writing – review & editing. **Günther Roman:** Formal analysis, Writing – review & editing. **Sandro Stucki:** Methodology, Writing – review & editing**. Feng Chen:** Methodology, Writing – review & editing. **Yong Ding:** Methodology, Writing – review & editing. **Wenqing Yan:** Methodology, Writing – review & editing. **Changsheng Wu:** Methodology, Writing – review & editing. **Laura Stricker:** Methodology, Writing – review & editing. **Ingo Burgert**: Funding acquisition, Writing – review & editing. **Zhong Lin Wang:** Resources, Writing – review & editing. **Guido Panzarasa** and **Dirk Hegemann**: Supervision, Resources, Project administration, Writing – review & editing.

Declaration of Competing Interest

The authors declare that they have no known competing financial interests or personal relationships that could have appeared to influence the work reported in this paper.

Data Availability

All data needed to evaluate the conclusions in the paper are present in the paper and/or the Supplementary Information. Additional data related to this paper may be requested from the authors.

Acknowledgments

Yong Ding received funding in the framework of the SNF Project "Hierarchical cellulose scaffolds for structural and functional gradient materials" (200021_184821/1). We thank T. Schnider for cutting the wood samples.

Appendix A. Supporting information

Supplementary data associated with this article can be found in the online version at doi:10.1016/j.nanoen.2022.107670.

References

[1] P. Farese, How to build a low-energy future, Nature 488 (2012) 275–277.
[2] T. Li, Y. Zhai, S. He, W. Gan, Z. Wei, M. Heidarinejad, D. Dalgo, R. Mi, X. Zhao, J. Song, J. Dai, C. Chen, A. Aili, A. Vellore, A. Martini, R. Yang, J. Srebric, X. Yin, L. Hu, A radiative cooling structural material, Science 364 (2019) 760–763.
[3] Y. Zhou, S. Wang, J. Peng, Y. Tan, C. Li, F. Boey, Y. Long, Liquid thermo-responsive smart window derived from hydrogel, Joule 4 (2020) 2458–2474.
[4] S.B. Sadineni, S. Madala, R.F. Boehm, Passive building energy savings: a review of building envelope components, Renew. Sust. Energ. Rev. 15 (2011) 3617–3631.
[5] C. Ballif, L.E. Perret-Aebi, S. Lufkin, E. Rey, Integrated thinking for photovoltaics in buildings, Nat. Energy 3 (2018) 438–442.
[6] B. Svetozarevic, M. Begle, P. Jayathissa, S. Caranovic, R.F. Shepherd, Z. Nagy, I. Hischier, J. Hofer, A. Schlueter, Dynamic photovoltaic building envelopes for adaptive energy and comfort management, Nat. Energy 4 (2019) 719.
[7] J. Yan, Y. Yang, P. Elia Campana, J. He, City-level analysis of subsidy-free solar photovoltaic electricity price, profits and grid parity in China, Nat. Energy 4 (2019) 709–717.
[8] J.G. Sun, K. Tu, S. Büchele, S.M. Koch, Y. Ding, S.N. Ramakrishna, S. Stucki, H. Guo, C. Wu, T. Keplinger, J. Pérez-Ramírez, I. Burgert, G. Panzarasa, Functionalized wood with tunable tribopolarity for efficient triboelectric nanogenerators, Matter 4 (2021) 3049–3066.
[9] G. Panzarasa, I. Burgert, Designing functional wood materials for novel engineering applications, Holzforschung 76 (2022) 211–222.
[10] Y.Y. Li, et al., Philos. T. R. Soc. A 376 (2018).
[11] T. Li, et al., Adv. Energ. Mater. 6 (2016).
[12] M.W. Zhu, et al., Adv. Mater. 28 (2016).
[13] T. Li, J. Song, X. Zhao, Z. Yang, G. Pastel, S. Xu, C. Jia, J. Dai, C. Chen, A. Gong, F. Jiang, Y. Yao, T. Fan, B. Yang, L. Wagberg, R. Yiang, L. Hu, Anisotropic, lightweight, strong, and super thermally insulating nanowood with naturally aligned nanocellulose, Sci. Adv. 4 (2018) eaar3724.
[14] F.R. Fan, Z.Q. Tian, Z. Lin Wang, Flexible triboelectric generator, Nano Energy 1 (2012) 328–334.
[15] Z.L. Wang, J. Chen, L. Lin, Progress in triboelectric nanogenerators as a new energy technology and self-powered sensors, Energ. Environ. Sci. 8 (2015) 2250–2282.
[16] J.Q. Xiong, et al., Nat. Commun. 9 (2018) 10138.
[17] J.G. Sun, T.N. Yang, I.S. Kuo, J.M. Wu, C.Y. Wang, L.J. Chen, A leaf-molded transparent triboelectric nanogenerator for smart multifunctional applications, Nano Energy 32 (2017) 180–186.
[18] J.G. Sun, T.N. Yang, C.Y. Wang, L.J. Chen, A flexible transparent one-structure tribo-piezo-pyroelectric hybrid energy generator based on bio-inspired silver nanowires network for biomechanical energy harvesting and physiological monitoring, Nano Energy 48 (2018) 383–390.
[19] Y. Zi, J. Wang, S. Wang, S. Li, Z. Wen, H. Guo, Z.L. Wang, Effective energy storage from a triboelectric nanogenerator, Nat. Commun. 7 (2016) 10987.
[20] C. Lee, S. Yang, D. Choi, W. Kim, J. Kim, J. Hong, Chemically surface-engineered polydimethylsiloxane layer via plasma treatment for advancing textile-based triboelectric nanogenerators, Nano Energy 57 (2019) 353–362.
[21] G. Wimmers, Wood: a construction material for tall buildings, Nat. Rev. Mater. 2 (2017) 17051.
[22] A.F. Diaz, R.M. Felix-Navarro, A semi-quantitative tribo-electric series for polymeric materials: the influence of chemical structure and properties, J. Electro 62 (2004) 277–290.

[23] J. Luo, Z. Wang, L. Xu, A.C. Wang, K. Han, T. Jiang, Q. Lai, Y. Bai, W. Tang, F. R. Fan, Z.L. Wang, Flexible and durable wood-based triboelectric nanogenerators for self-powered sensing in athletic big data analytics, Nat. Commun. 10 (2019) 5147.
[24] S. Hao, J. Jiao, Y. Chen, Z.L. Wang, X. Cao, Natural wood-based triboelectric nanogenerator as self-powered sensing for smart homes and floors, Nano Energy 75 (2020), 104957.
[25] J. Bang, I.K. Moon, Y.P. Jeon, B. Ki, J. Oh, Fully wood-based green triboelectric nanogenerators, Appl. Surf. Sci. 567 (2021), 150806.
[26] C. He, W. Zhu, B. Chen, L. Xu, T. Jiang, C.B. Han, G.Q. Gu, D. Li, Z.L. Wang, Smart floor with integrated triboelectric nanogenerator as energy harvester and motion sensor, ACS Appl. Mater. Inter. 9 (2017) 26126–26133.
[27] C. Zhang, J. Mo, Q. Fu, Y. Liu, S. Wang, S. Nie, Wood-cellulose-fiber-based functional materials for triboelectric nanogenerators, Nano Energy 81 (2021), 105637.
[28] C. Cai, J. Mo, Y. Lu, N. Zhang, Z. Wu, S. Wang, S. Nie, Integration of a porous wood-based triboelectric nanogenerator and gas sensor for real-time wireless food-quality assessment, Nano Energy 83 (2021), 105833.
[29] X. Yang, G. Zhu, S. Wang, R. Zhang, L. Lin, W. Wu, Z.L. Wang, A self-powered electrochromic device driven by a nanogenerator, Energ. Environ. Sci. 5 (2012) 9462–9466.
[30] W. Qiu, Y. Feng, N. Luo, S. Chen, D. Wang, Sandwich-like sound-driven triboelectric nanogenerator for energy harvesting and electrochromic based on Cu foam, Nano Energy 70 (2020), 104543.
[31] M.H. Yeh, L. Lin, P.K. Yang, Z.L. Wang, Motion-driven electrochromic reactions for self-powered smart window system, ACS Nano 9 (2015) 4757–4765.
[32] W. Seung, M.K. Gupta, K.Y. Lee, K.S. Shin, J.H. Lee, T.Y. Kim, S. Kim, J. Lin, J. H. Kim, S.W. Kim, Nanopatterned textile-based wearable triboelectric nanogenerator, ACS Nano 9 (2015) 3501–3509.
[33] B.K. Yun, J.W. Kim, H.S. Kim, K.W. Jung, Y. Yi, M.S. Jeong, J.H. Ko, J.H. Jung, Base-treated polydimethylsiloxane surfaces as enhanced triboelectric nanogenerators, Nano Energy 15 (2015) 523–529.
[34] M. Muthu, R. Pandey, X. Wang, A. Chandrasekhar, I.A. Palani, V. Singh, Enhancement of triboelectric nanogenerator output performance by laser 3D-Surface pattern method for energy harvesting application, Nano Energy 78 (2020), 105205.
[35] G. Avramidis, E. Hauswald, A. Lyapin, H. Militz, W. Viöl, A. Wolkenhauer, Plasma treatment of wood and wood-based materials to generate hydrophilic or hydrophobic surface characteristics, Wood Mater. Sci. Eng. 4 (2009) 52–60.
[36] L. Xie, Z. Tang, L. Jiang, V. Breedveld, D.W. Hess, Creation of superhydrophobic wood surfaces by plasma etching and thin-film deposition, Surf. Coat. Tech. 281 (2015) 125–132.
[37] G.G. Volokitin, N.K. Skripnikova, V.A. Sinitsyn, O.G. Volokitin, V.V. Shekhovtsov, S.P. Vaschenko, V.I. Kuz'min, Plasma treatment of wood, Thermophys. Aeromech. 23 (2016) 119–124.
[38] Y. Ding, K. Tu, I. Burgert, T. Keplinger, Janus wood membranes for autonomous water transport and fog collection, J. Mater. Chem. A 8 (2020) 22001–22008.
[39] J.S.G. de Camargo, et al., Mater. Res-Ibero-Am. J. 20 (2017) 842–850.
[40] I. Chun, A. Efremov, G.Y. Yeom, K.H. Kwon, A comparative study of CF4/O2/Ar and C4F8/O2/Ar plasmas for dry etching applications, Thin Solid Films 579 (2015) 136–143.
[41] D. Hegemann, H. Brunner, C. Oehr, Plasma treatment of polymers for surface and adhesion improvement, Nucl. Instrum. Meth. B 208 (2003) 281–286.
[42] S. Lee, Y. Lee, D. Kim, Y. Yang, L. Lin, Z.-H. Lin, W. Hwang, Z.L. Wang, Triboelectric nanogenerator for harvesting pendulum oscillation energy, Nano Energy 2 (2013) 1113–1120.
[43] S.J. Park, et al., Sci. Rep. -Uk 5 (2015) 1–7.
[44] C. Xu, Y. Zi, A.C. Wang, H. Zou, Y. Dai, X. He, P. Wang, Y.C. Wang, P. Feng, D. Li, Z. L. Wang, On the electron-transfer mechanism in the contact-electrification effect, Adv. Mater. 30 (2018), 1706790.
[45] Z.L. Wang, A.C. Wang, On the origin of contact-electrification, Mater. Today 30 (2019) 34–51.
[46] Y.H. Zhou, et al., Cell Rep. Phys. Sci. 1 (2020).
[47] S. Li, Y. Fan, H. Chen, J. Nie, Y. Liang, X. Tao, J. Zhang, X. Chen, E. Fu, Z.L. Wang, Manipulating the triboelectric surface charge density of polymers by low-energy helium ion irradiation/implantation, Energ. Environ. Sci. 13 (2020) 896–907.
[48] J. Rice, et al., Wood Fiber Sci. 38 (2006) 644–659.
[49] I. Kim, H. Jeon, D. Kim, J. You, D. Kim, All-in-one cellulose based triboelectric nanogenerator for electronic paper using simple filtration process, Nano Energy 53 (2018) 975–981.
[50] X. Kang, C. Pan, Y. Chen, X. Pu, Boosting performances of triboelectric nanogenerators by optimizing dielectric properties and thickness of electrification layer, Rsc Adv. 10 (2020) 17752–17759.
[51] A. Ahmed, I. Hassan, T. Ibn-Mohammed, H. Mostafa, I.M. Reaney, L. Koh, J. Zu, Z. L. Wang, Environmental life cycle assessment and techno-economic analysis of triboelectric nanogenerators, Energ. Environ. Sci. 10 (2017) 653–671.
[52] J.C. Kelly, M. Wang, Q. Dai, O. Winjobi, Energy, greenhouse gas, and water life cycle analysis of lithium carbonate and lithium hydroxide monohydrate from brine and ore resources and their use in lithium ion battery cathodes and lithium ion batteries, Resour. Conserv. Recycl. 174 (2021), 105762.
[53] J. Trieschmann, D. Hegemann, Plasma polymerization at different positions in an asymmetric ethylene discharge, J. Phys. D. Appl. Phys. 44 (2011), 475201.
[54] K. Tu, X. Wang, L. Kong, H. Chang, J. Liu, Fabrication of robust, damage-tolerant superhydrophobic coatings on naturally micro-grooved wood surfaces, RSC Adv. 6 (2016) 701–707.

Jianguo Sun received his B.S and M.S degrees from Department of Materials Science and Engineering at Zhengzhou university (2014) and National Tsing Hua University (2016), respectively. He received his Ph.D. degree from Wood Materials Science Group at Department of Civil, Environmental and Geomatic Engineering, ETH Zürich (2021). His research interests include wood modification, tribo- and/or piezoelectric nanogenerators, and energy-efficient building materials.

Kunkun Tu is a postdoctoral researcher in the Wood Materials Science group of ETH Zürich. She obtained her BSc and MSc degrees at Nanjing Forestry University (2014) and Chinese Academy of Forestry (2017), respectively. Besides, she received her PhD degree from ETH Zürich (2021). Her research interests focused on the design, synthesis, and characterization of functional wood materials, and exploring their potential applications in CO_2 adsorption, energy harvesting and conversion, and catalysis.

Sophie Marie Koch graduated from Maastricht University, Netherlands, with a Master of Science degree in Bio-based Materials. In her current PhD research, she focuses on developing novel delignified wood composites by using a broad range of polymeric matrices. She is particularly interested in the characterization of wood's structural intricacies on a micro- and nanometer scale and their interplay with the infiltrating matrices.

Roman Günther obtained a Master of Science in Advanced Materials and Processes from the Friedrich Alexander University, Erlangen, Germany in 2016. In 2017 he joined the Zurich University of Applied Science in Winterthur, Switzerland, in the laboratory of adhesives and polymers as a research assistant. 2019 he started his joint Ph.D. studies in a corporation with ETH Zurich, Switzerland. His research focuses on polymeric surface modification and characterization and new reversible bonding technologies for incompatible polymers.

Sandro Stucki received his B.S in Food Technology from the Zurich University of Applied Sciences (ZHAW) and his M.S. degree in Food Science from the Swiss Federal Institute of Technology (ETHZ). He is currently a Ph.D. candidate under the supervision of Ingo Burgert in the Wood Material Science Group at the Swiss Federal Institute of Technology (ETHZ) in Switzerland and the Swiss Federal Institute of Technology (Empa). His research interests are in wood adhesion, with a focus on adhesion primers and surface functionalizations for improved wood bonding.

Feng Chen received his Ph.D. in early 2021 from Aalto University (Finland) and worked as a visiting scholar at CEMEF, Mines ParisTech, PSL Research University (France) from 2017 to 2020. After his Ph. D. he worked as postdoctoral researcher in the Wood Materials Science Group at ETH Zurich (Switzerland) for one year and finished in 2022. Presently, he is a researcher at Jianghan University (Wuhan, China). His research covers fundamental aspects of dissolution/swelling of multiscale cellulosic fibers in ionic liquid-water systems as well as applied aspects of reassembly of multiscale cellulose/wood for high-ends applications.

Yong Ding started her doctoral study in the Wood materials Science group of ETH Zürich in 2019. She received her B.Eng. degree in 2015 and M.Sc. degree in 2018 from Tianjin University. Her research focuses on exploiting the inherent properties of wood and combining them with advanced modification and processing techniques. She is interested in developing functional wood materials with application potential *e.g.* for autonomous water transport and smart building materials.

Wenqing Yan studied polymer science at the University of Freiburg (Germany), where she received her master's degree in 2017. She carried out her Ph.D. in the Laboratory for Surface Science and Technology in the Department of Materials at ETH Zürich. Since 2021, she has been a postdoctoral researcher in the Wood Materials Science Group at Department of Civil, Environmental and Geomatic Engineering, ETH Zürich. Her research interests focus on green and sustainable polymer synthesis, wood membrane, osmotic energy conversion.

Laura Stricker got her PhD in Physics at the University of Twente (NL), working on cavitation and sonochemistry. After investigating active droplets as a Marie Curie postdoctoral fellow at the Max Planck Institute for Dynamics and Self-Organization in Göttingen (DE), she currently works in the Department of Materials at ETHZ since 2017. Her main research focus are phase transitions in complex systems, pattern formation, modelling of transport phenomena, numerical solutions of PDEs and image analysis, with the ultimate goal of the development and characterization of novel active and sustainable materials.

Ingo Burgert received a diploma in Wood Science and Technology at the University of Hamburg, Germany, in 1995, followed by a doctoral degree in 2000. From 2000–2003 he was postdoc at the University of Natural Resources and Life Sciences (BOKU), Vienna, Austria. From 2003–2011, he was a research group leader at the Max Planck Institute of Colloids and Interfaces, in the Department of Biomaterials, Potsdam, Germany. Since 2011 he has been a professor of Wood Materials Science at ETH - Swiss Federal Institute of Technology, Zurich and group leader at Empa - Swiss Federal Laboratories for Materials Science and Technology, Dübendorf, Switzerland.

Guido Panzarasa received his PhD in Chemical Sciences in 2016 from the University of Eastern Piedmont "Amedeo Avogadro" (Italy). After a brief research assistantship at Montanuniversität Leoben (Austria), he came to Switzerland as a postdoctoral researcher first at Empa (from 2016 to 2018) and then at ETH Zürich (from 2018 to 2020). In 2020 he was promoted group leader in the Wood Materials Science Laboratory led by Prof. Dr. Ingo Burgert at ETH Zürich. His research interests are highly interdisciplinary, spanning from polymer science to nanochemistry, from systems chemistry to active and adaptive wood materials.